Carbon 127 (2018) 688–698

Contents lists available at ScienceDirect

Carbon

journal homepage: www.elsevier.com/locate/carbon

Next generation membranes —using tailored carbon

Oishi Sanyal, Chen Zhang, Graham B. Wenz, Shilu Fu, Nitesh Bhuwania, Liren Xu, Meha Rungta, William J. Koros*

School of Chemical and Biomolecular Engineering, Georgia Institute of Technology, Atlanta, GA 30332, USA

ARTICLE INFO

Article history:
Received 20 August 2017
Received in revised form
28 October 2017
Accepted 11 November 2017
Available online 15 November 2017

ABSTRACT

Carbon molecular sieve (CMS) membranes are a special class of nanoporous membranes with angstrom-level molecular discrimination properties, which make them appealing for separating a wide spectrum of gas-pairs. The mechanism of pyrolysis by which a polymer coil is transformed into these rigid sieves is complex; however, we present a framework that can explain this transformation. Representative polymer precursors and pyrolysis conditions are discussed that yield attractive CMS membrane separation performance for extremely challenging gas pairs. Control of penetrant motions in the diffusion activated state, reflected in the entropy of activation of subtly different penetrants, enables the attractive diffusion selectivity of such membranes. This control, virtually absent even in rigid state-of-the-art polymeric membranes, makes CMS materials extraordinarily attractive. Moreover, unlike other rigid sieving materials, CMS membranes have the added advantage of being processable into highly productive, flexible hollow fibers with good mechanical properties and long-term stability under constant gas feeds. In this article, we also identify some key areas of CMS which would greatly benefit from expertise from other fields like computation or materials characterization that can potentially complement transport-based studies.

1. Introduction

Of the many forms of carbon, amorphous allotropes are arguably the most diverse and complicated; moreover, other atoms such as O and N present in the structures, further increase their complexity. Readers of *Carbon* include many sophisticated materials characterization experts, covering an impressive array of techniques such as Raman [1,2], FT-IR [3], X-ray photoelectron spectroscopy (XPS) [4,5], Wide angle X-Ray diffraction (WAXD) [6,7], Small angle X-ray scattering (SAXS) [8], CO_2 porosimetry [9,10], positron annihilation spectroscopy (PALS) [11,12] and transmission electron microscopy (TEM) [13,14]. Another group of readers includes those exploring new materials useful in advanced solutions to important practical problems. Our group is part of this second set, and we bring experience in material processing to create economical large-scale devices suitable for separating some of the most difficult feed mixtures, conventionally handled by energy intensive processes.

The array of sophisticated characterization techniques noted above are valuable for all carbon types, but transport characterizations offer additional unique insights that should also be complemented with traditional techniques when possible. This point will be illustrated by considering *carbon membranes* derived from well-defined polymer precursors such as those in Table 1.

Besides expanding the fundamental range of materials available to the carbon community, such membranes have the potential to solve extremely challenging separation problems more efficiently than other currently available materials. Examples of such challenging problems include separation of CO_2 and N_2 from CH_4 for purification and economical use of natural gas. Other examples include olefin-paraffin pairs like C_3H_6/C_3H_8 and C_2H_4/C_2H_6, which currently rely upon very energy intensive distillation processes. All of the above cases require discrimination of gas molecules differing by less than 1 Å in their minimum dimensions,Δ, as shown in Fig. 1.

Indeed, the special carbon materials able to perform these separations are referred to as “carbon molecular sieves” (CMS) to reflect their unique properties and comprise the focus of this perspective article. These rigid molecular sieves are the products of controlled high temperature pyrolysis of well-defined polymer precursors, in our case polyimides. We feel that *Carbon* provides the ideal forum to discuss creation and characterization of this fascinating group of materials. Since not all readers of *Carbon* are membrane scientists, clarification of a few basic terms is useful. The

* Corresponding author.
E-mail address: wjk@chbe.gatech.edu (W.J. Koros).

https://doi.org/10.1016/j.carbon.2017.11.031
0008-6223/

Table 1
Chemical structures of some well-defined CMS precursors ([15–17]).

Polymer	Repeat structure
Matrimid® (BTDA-DAPI)	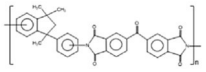
6FDA: BPDA-DAM (1:1)	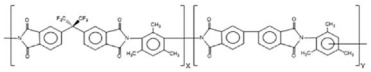
6FDA-DETDA: DABA (3:2)	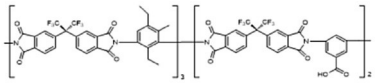

permeability coefficient (or more commonly Permeability), P_A of a component, A is defined by Eq. (1).

$$P_A = \frac{N_A \cdot l}{\Delta p_A} \tag{1}$$

where N_A is the steady-state flux of penetrant A through a membrane of thickness l caused by the transmembrane partial pressure (fugacity) difference Δp_A.

The permeability is an intrinsic material property equal to the product of the diffusion coefficient (D_A) and sorption coefficient ($\mathbb{S}_A$) of penetrant A in the membrane, so $P_A = D_A\mathbb{S}_A$. The sorption coefficient, ($\mathbb{S}_A$) equals the concentration of sorbed penetrant A, normalized by the equilibrium pressure. Sorption in CMS typically follows the Langmuir isotherm model as expressed in Eq. 2.

$$\mathbb{S}_A = \frac{C_A}{p_A} = \frac{C'_{HA} \cdot b_A}{1 + b_A p_A} \tag{2}$$

where C_A is the equilibrium uptake of gas A under equilibrium pressure p_A, C'_{HA} and b_A are Langmuir constants, C'_{HA} being the Langmuir hole-filling capacity and b_A the Langmuir affinity constant.

By extension, the permselectivity of a membrane for component A = CO_2 *vs.* B= CH_4 equals, $P_A/P_B = (\alpha_{AB})_D(\alpha_{AB})_S$, where $(\alpha_{AB})_D = D_A/D_B$ and $(\alpha_{AB})_S = \mathbb{S}_A/\mathbb{S}_B$. [The $\mathbb{S}$ – symbol is used to denote sorption coefficient while entropy, which is discussed later, is denoted by $S^{\dagger}$.] In the above cases, component A is the smallest member of the respective pairs, e.g. CO_2, N_2, C_3H_6 and C_2H_4. Permeation, diffusion and sorption characterizations complement other sophisticated characterization techniques noted above, and encouraging this complementarity is a goal of this perspective article.

2. Metamorphosis of random coils into rigid molecular sieves

The pyrolysis process by which a polymer precursor is transformed into a CMS material is obviously complex. Identifying steps in CMS material property transformation from the precursor and the pyrolysis process responsible for this transformation is a good starting point for all the discussions that follow. Such materials are envisioned to comprise aromatized strands arranged to form plates, which are further organized into amorphous cellular structures [18]. The slits between the strands, referred to as ultramicropores (<7 Å), allow precise angstrom-level discrimination between penetrant molecules, thereby regulating the sieving behavior of the membranes. The voids between imperfectly arranged carbon plates, referred to as micropores (7–20 Å), act as the sorption sites and determine the diffusion jump lengths for gas molecules. The disrupted turbostratic structure shown in Fig. 2 illustrates the key features described above. The mechanism to form CMS from random polymer coils is discussed in detail with respect to Fig. 3.

In this perspective, we will primarily focus on the three polymeric precursors in Table 1 that have already been shown to provide attractive CMS properties. The CMS derived from the 6FDA-DETDA:DABA precursor provides the highest gas permeability, followed by the CMS from 6FDA:BPDA-DAM, while Matrimid®-derived CMS shows the lowest permeability. In general, relationships between precursor and CMS properties are complicated [19] due to the significant rearrangements occurring during pyrolysis, so this topic is an area of opportunity for carbon scientists.

CMS materials have the potential for use in large modular devices with thousands of square meters of membranes. Before discussing complex asymmetric CMS forms with thin selective layers needed for such devices, insights on thicker (50 μm) CMS derived from simple polymer precursor films should be reviewed [20]. Fig. 3 and the associated discussion adapted from Ref. [20] summarize our vision of such dense film transformation processes.

Irrespective of the precursor structures, pyrolytic transformation to useful CMS structures involves formation of disordered aromatic structures sharing some common features. For all the topics discussed in this perspective, we focus only on pyrolysis carried out under non-vacuum, essentially inert atmosphere.

This process occurs in three periods: (i) thermal ramp; (ii) thermal soak; (iii) cooling with maximum temperatures usually <1000 °C to provide attractive CMS gas permeabilities. In such a three-step pyrolysis, transformation of a random polymer coil into a functional CMS material occurs with evolution of volatiles. For the 6FDA:BPDA-DAM precursor shown in Table 1, CF_3H, HF, CO_2, CO and H_2 are evolved during the thermal ramp [21]. In this thermal ramping step, a highly aromatic strand type structure, like that represented in Fig. 3(ii), forms. Further aromatization, while maintaining considerable nitrogen in the strand [22–26], is apparent from elemental analysis [20]. For the other precursors shown in Table 1, different but similarly rigid aromatic structures are believed to result during the thermal ramp period where subsequent organizational steps outlined below ultimately result in a specific CMS material.

The semi-flexible random coil 6FDA:BPDA-DAM polyimide loses <40% of its weight, even up to 800 °C. During this stage, a high

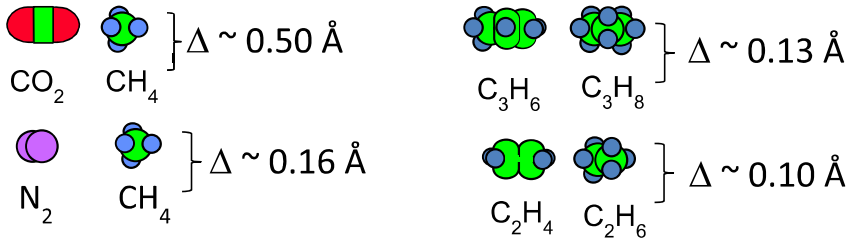

Fig. 1. Challenging high pay-off gas pairs benefitting from CMS size and shape selectivity. (A colour version of this figure can be viewed online.)

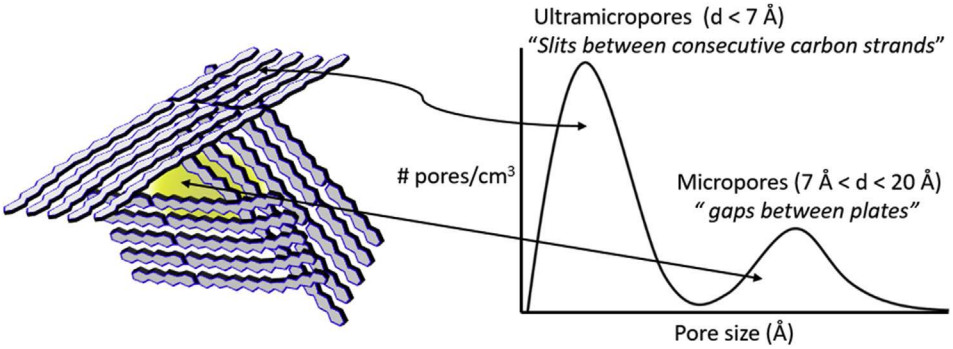

Fig. 2. Turbostratic carbon structure with its idealized micropore and ultramicropore structure. (A colour version of this figure can be viewed online.)

molecular weight rigid structure is created, which faces a *solid state packing problem*. A similar problem is encountered during transformation of a high molecular weight cellulosic precursor. In fact, any entangled semi-flexible precursor undergoing aromatization and extreme linearization will tend to experience sufficient localized stresses to cause scissions along their backbones, illustrated in Fig. 3(i) and (ii). Backbone scissions during the temperature ramp to the final pyrolysis temperature allow aromatization to proceed while producing shorter, more mobile structural strands. However, such an array of strands still faces *a packing problem*. By organizing into more packable entities such as plates, this packing problem is solved, as in the case of liquid crystal materials [27]. Further entropically-driven organization of the plates (Fig. 3(iii)) proceeds in parallel with the aromatization process. Alignment of strands during the temperature ramp phase of the pyrolysis avoids excluded volume present within a "random" phase packing of

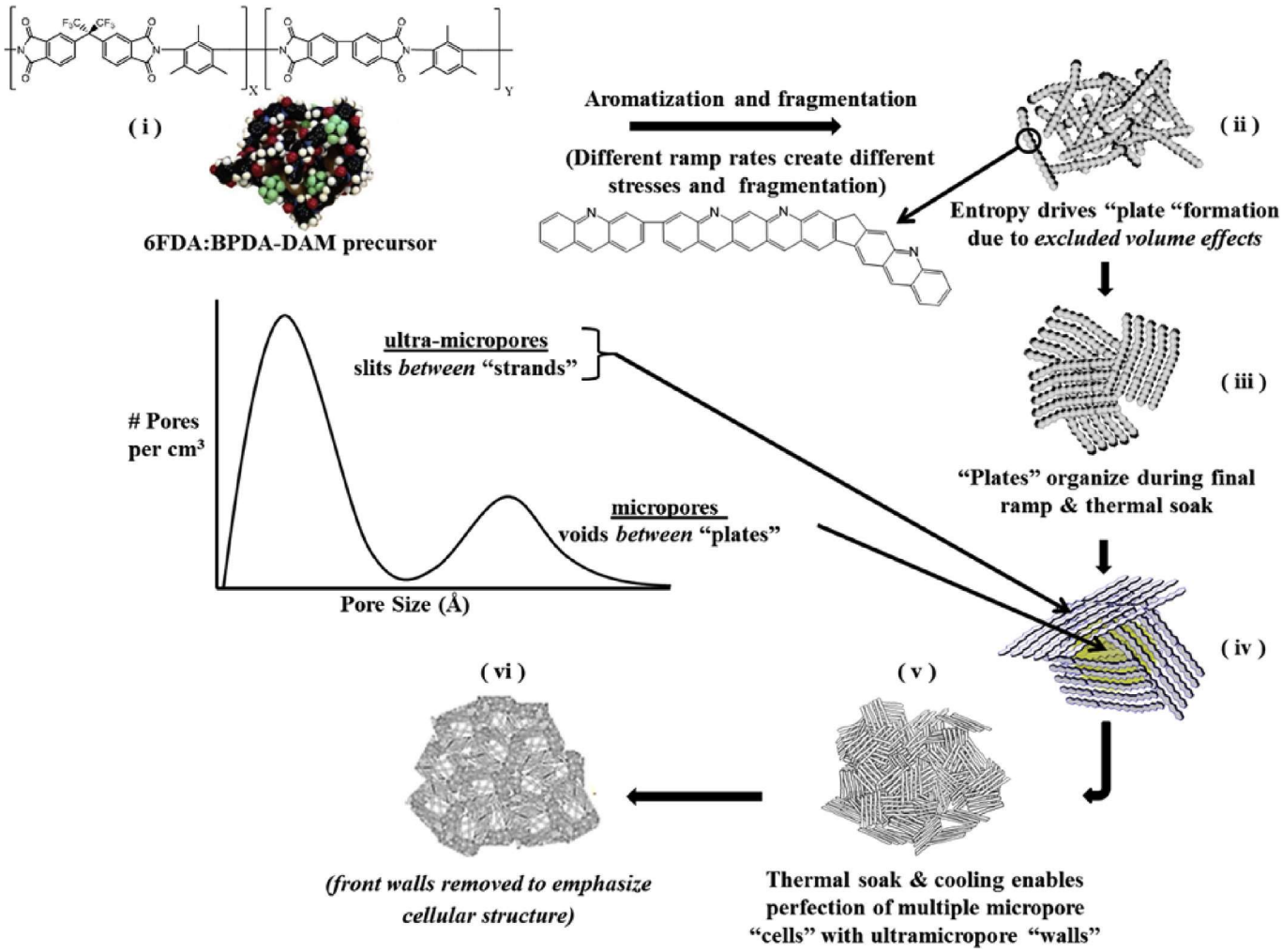

Fig. 3. Envisioned steps in transformation from random coil precursor polyimide to organized amorphous CMS material with bimodal distribution of micro pores with ultramicropores(Reproduced with permission from Ref. [20]). (A colour version of this figure can be viewed online.)

strands (Fig. 3(ii)) and also provides an increased number of possible packing states of lateral entities—as in the case of liquid crystals [27]. Ultimately, lateral linkages due to reactive consolidation of some neighboring strands may occur with evolution of molecular H_2 at higher temperatures. Nevertheless, an amorphous long-range nature exists, since kinetic restrictions hinder organization within the plates themselves and cause long range stacking defects between plates during "ramp" and "soak" periods where mobility is highest. An idealized micropore "cell" with imperfectly packed sides comprising imperfectly organized strands is illustrated in Fig. 3(iv). Ongoing formation of many neighboring cells in an idealized CMS structure may occur during thermal soak and cooling after pyrolysis, as illustrated in Fig. 3(iv)–(vi). Coalescence of micropore "cells" (Fig. 3(iv)) enables sharing of ultramicropore "walls" between "cells", thereby creating the cellular structure illustrated in Fig. 3(vi), with the front ultramicropore "walls" removed to view the cellular structure. Such an amorphous CMS, with micropores separated by ultramicropores in the micropore plate walls, has *molecular sieving* properties. The above discussion is useful not only to envision the formation of the polyimide-derived CMS, but also to understand how controlling processing conditions like pyrolysis atmosphere, thermal ramp rate, soak time etc. [28] and post-processing affect final CMS membrane performance.

Fu et al., studied the performance of four different 6FDA-based precursors and their corresponding CMS properties [19]. Increasing fractional free volumes of the *polymer precursors* correlated with increased precursor permeability; however, the resulting *CMS performance* bore no predictable correlation with the precursor free volume. In other words, a high free volume precursor did not simply translate into a highly permeable CMS. Of the four precursors studied by Fu et al., 6FDA-DETDA:DABA in Table 1 showed the second lowest *precursor permeability*; however, after pyrolyzing at 550 °C the resulting CMS from this material showed the highest CO_2 permeability. The observed CMS trend was attributed to –COOH groups in the DABA moieties [29], which cause crosslinking below the precursor glass transition temperature [30] before pyrolysis. Extending Fig. 3 to the case of 6FDA-DETDA:DABA, we hypothesize that the presence of crosslinks may lead to the formation of larger and more irregular fragments on going from (i) to (ii), which may also inhibit the organization of plates in the subsequent stages ((iii),(iv)), thereby increasing permeability.

3. Tailoring the sieve

Besides changing precursor type, the pyrolysis process itself offers tools to tailor the performance of the CMS membrane [31]. For example, increasing the final pyrolysis temperature leads to tightening of both micropores and ultramicropores [31–33]. Tightening of *ultramicropores* in Fig. 3 should increase the diffusion selectivity between two penetrants. On the other hand, reduction in *micropore* sizes reduces diffusion jump lengths (λ_i) across the micropores, thereby reducing diffusion coefficients. Moreover, reduced micropores would tend to reduce sorption coefficients ($\mathbb{S}_i$). Recalling that $P_A = D_A S_A$, one sees that permeability will drop, while permselectivity will rise with increasing pyrolysis temperature. An alternative strategy to increase diffusion selectivity with minimal effects on the diffusion jump length, λ_i, and sorption coefficient, $\mathbb{S}_i$, is clearly appealing. Addition of ppm levels of O_2 to an otherwise inert pyrolysis atmosphere may be such a technique [12]. [Fig. 4].

Fig. 4 illustrates "O_2 doping" decoration of the edges of ultramicropore slits to adjust diffusion selectivity. Moreover, O_2 doping was found to cause minimal differences in sorption capacities associated with micropores [12]. Ideally, therefore, diffusion jump lengths across micropores should be affected minimally compared to rate limiting jumps *through ultramicropores plates*.

Attractive permeability-selectivity trade-offs shown in Fig. 5, were observed for 6FDA-DETDA:DABA (3:2) CMS pyrolyzed at 550 °C with varying levels of O_2 (in ppm) [30]. In this case, as in the work of Kiyono [12], sorption coefficients remained essentially unaffected by the level of O_2 doping [10]. Diffusion coefficients and permeabilities were reduced moderately by lowering the number of available ultramicropores, so the tradeoff is desirable with higher selectivities. Specifically, ultramicropores could tolerate "tightening" without undue loss in those with adequate size to enable attractive D_{CO2} values. Since preservation of micropores provide high sorption and diffusion jump lengths, compared to the thermal tightening that occurs at high pyrolysis temperatures like 675 °C and 800 °C, O_2-doping helps to fine-tune the performance more precisely. Doping levels, however, needs optimization for different gas-pairs and CMS samples. For instance, the comparatively "tighter" 6FDA:BPDA-DAM CMS with a permeability of 7100 Barrers for 550 °C/UHP Argon pyrolysis, the optimum level is near 30 ppm [34]. Exceeding the 30 ppm limit leads to "over-doping" wherein both the productivity as well as selectivity are lost, and this was not observed even up to 50 ppm for the 6FDA-DETDA:DABA(3:2) case. Interestingly, the O_2-doping technique was not favorable for

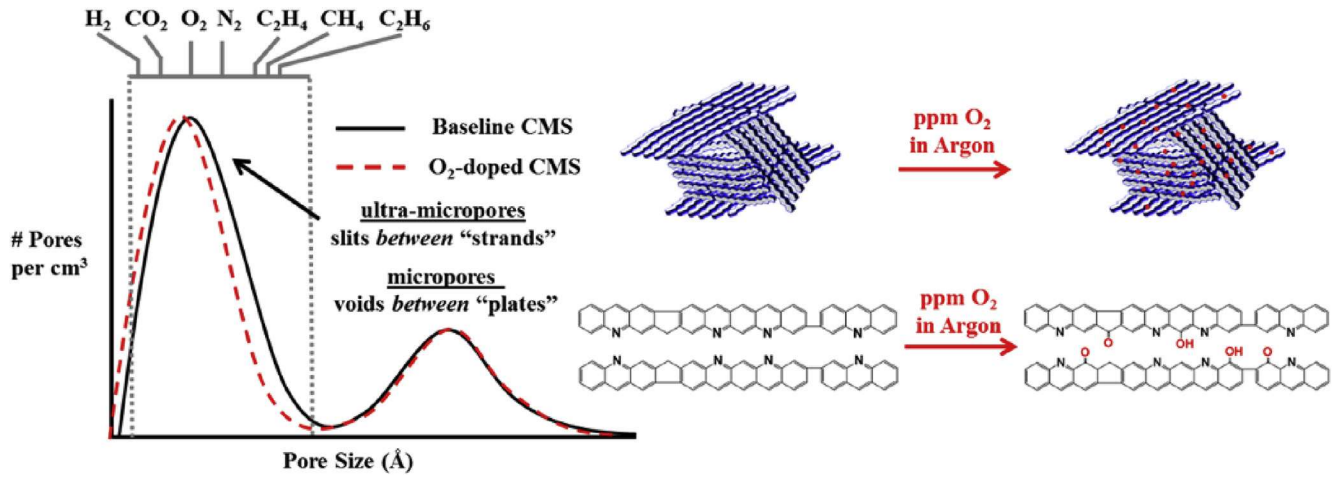

Fig. 4. Tuning of ultramicropore dimensions with O_2 doping (Reproduced with permission from Ref. [20]). (A colour version of this figure can be viewed online.)

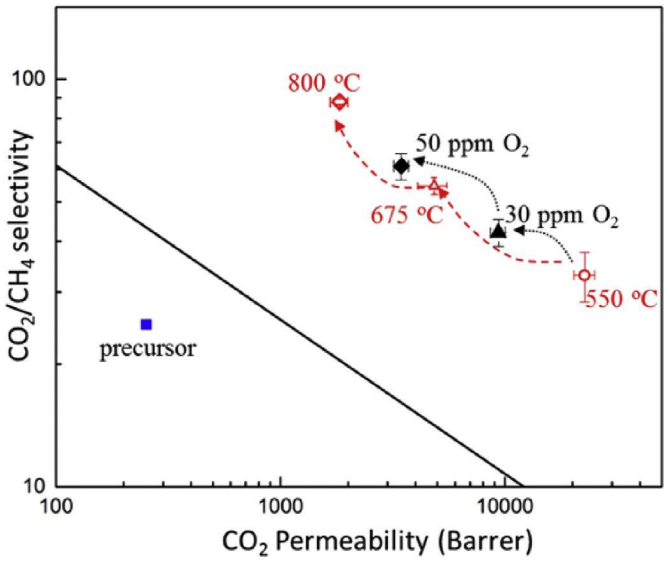

Fig. 5. O_2 doping of 6FDA/DETDA: DABA derived CMS for 550 °C pyrolysis *vs.* thermal tightening approach.(A colour version of this figure can be viewed online.)

Matrimid® CMS membranes, which are the least permeable among the three carbons discussed here with an intrinsic CO_2 permeability of 1000 Barrers at 550 °C/UHP Argon [35].

The even more challenging similar-sized gas-pair, C_2H_4/C_2H_6 ($\Delta = 0.1$ Å in Fig. 1) tends to show low diffusion selectivities in CMS materials pyrolyzed even at 675 °C under the usual inert environment. Doping the ultramicropores with an optimum level of just 10 ppm O_2 at 675 °C, raises the selectivity by ~30% with minimal reduction in permeability with respect to UHP Argon pyrolysis [20]. The detailed transport analyses supported by other relevant characterization techniques are part of ongoing work and will be reported separately.

4. What makes CMS special? - Entropic selectivity and processability

A broadly-applicable topic that motivated our initial interest in CMS materials involves the ability to exercise additional control on the diffusion transition state for similar-sized molecules in CMS membranes [36]. The CO_2/CH_4 pair discussed earlier fits this size-similar description; however, the C_2H_4/C_2H_6 pair mentioned above is an even more compelling case. The C_2 pair also has intrinsically low sorption selectivity due to similar critical temperatures, in the absence of complexing carrier. Such carriers have not proven to be stable in long term use, so permselectivities must rely almost entirely upon size and shape-based molecular discriminations. Penetrants execute size-dependent diffusion-selective jumps, moderated by the activation energy (or more precisely activation enthalpy) required to execute jumps. This energetically based molecular discrimination process is called "energetic selectivity" and this tool appears to be reaching a point of diminishing returns [37]. Fortunately, the transition state theory of diffusion provides a detailed expression for diffusion selectivity in Eq (3), which shows an additional factor, termed "*entropic selectivity*" [37]. The transition state representation of diffusion selectivity includes a quadratic ratio of jump lengths of component A *vs.* B, multiplied by the exponential difference in free energies of activation:

$$\left(\frac{D_A}{D_B}\right) = \frac{\lambda_A^2}{\lambda_B^2}\exp\left(\frac{-\Delta G_{D,AB}^{\dagger}}{RT}\right) = \frac{\lambda_A^2}{\lambda_B^2}\exp\left(\frac{-\Delta\left(H_{D,AB}^{\dagger} - TS_{D,AB}^{\dagger}\right)}{RT}\right)$$
$$= \frac{\lambda_A^2}{\lambda_B^2}\underbrace{\exp\left(\frac{-\Delta\left(H_{D,AB}^{\dagger}\right)}{RT}\right)}_{\text{Energetic selectivity}}\underbrace{\exp\left(\frac{+\Delta\left(S_{D,AB}^{\dagger}\right)}{R}\right)}_{\text{Entropic– selectivity}} \quad (3)$$

The jump lengths between sorption sites are effectively identical for A & B in precisely molecularly sieving matrices, so the diffusion selectivity equals the product of the exponential energetic and entropic selectivity terms. CMS materials have the ability to exert entropic selectivity by constraining *translational, rotational and vibrational activated state degrees of freedom of the rejected component of similar-sized gas pairs* [38]. Such constraints reduce diffusion coefficients of the rejected component greatly, while maintaining high diffusion coefficients of the slightly more compact member in the above-mentioned important penetrant pairs. Relatively easy processability into *high flux asymmetric* molecular sieving structures, combined with *reasonable mechanical properties discussed later*, makes CMS unique among other high-performing rigid microporous membrane materials (e.g. zeolites, metal-organic frameworks etc.).

Studies by Rungta et al., show that for the C_2H_4/C_2H_6 pair, increases in selectivity occur as the pyrolysis temperature is increased to 675 °C from 550 °C under inert atmosphere for both Matrimid® and 6FDA: BPDA-DAM precursors [31,39]. This analysis is best understood in terms of two important limiting cases ("loose" and "tight" slit in the diffusion transition state as discussed by Rungta [40] (see Fig. 6)). It should be noted that the "slits" referred to here comprise ultramicropores formed between adjacent carbon strands that are described in Figs. 2 and 3.

(i) **"Loose" Slit:** In this case, the CMS pore structure is "loose" due to lower pyrolysis temperature or lack of O_2 doping, so free rotation of C_2H_4 and C_2H_6 is possible around both the x and y axes in the transition state. The entropic factor is essentially unity, with less advantage *vs.* case (ii) below.

(ii) **"Tight" Slit:** In this case, the CMS pore structure is "tighter" (at higher pyrolysis temperature or optimum O_2 doping) which allows rotation of C_2H_4 around both x and y axes, but in this case restricted rotation of C_2H_6 around both the x and y axes exists, while only allowing it to rotate around the y axis. In this case, the entropic factor can be shown to be as high as 31 [40].

The "tight slit "case with high entropic selectivity factor is clearly the preferred choice to obtain attractive diffusion selectivities. In this case, the lost degrees of rotational freedom of C_2H_6 may be transformed into additional vibrational degrees of freedom. In fact, due to the complicated shapes of C_2H_4 and C_2H_6, entropic advantages may depend on more subtle configurational differences of the molecules, rather than an absolute total loss of a degree of freedom. Similar, but considerably more complicated theoretical analyses, like that for the C_2 pair are possible for the C_3H_6/C_3H_8 pair. The ability to tune the entropic factor has also proved to be extremely valuable for separating N_2 from CH_4, which otherwise would be very difficult simply based on size discrimination. As reported by Ning et al., for Matrimid® CMS pyrolyzed at 800 °C; the contribution of the energetic factor to the diffusion selectivity of N_2/CH_4 was found to be less than unity but the entropic factor was

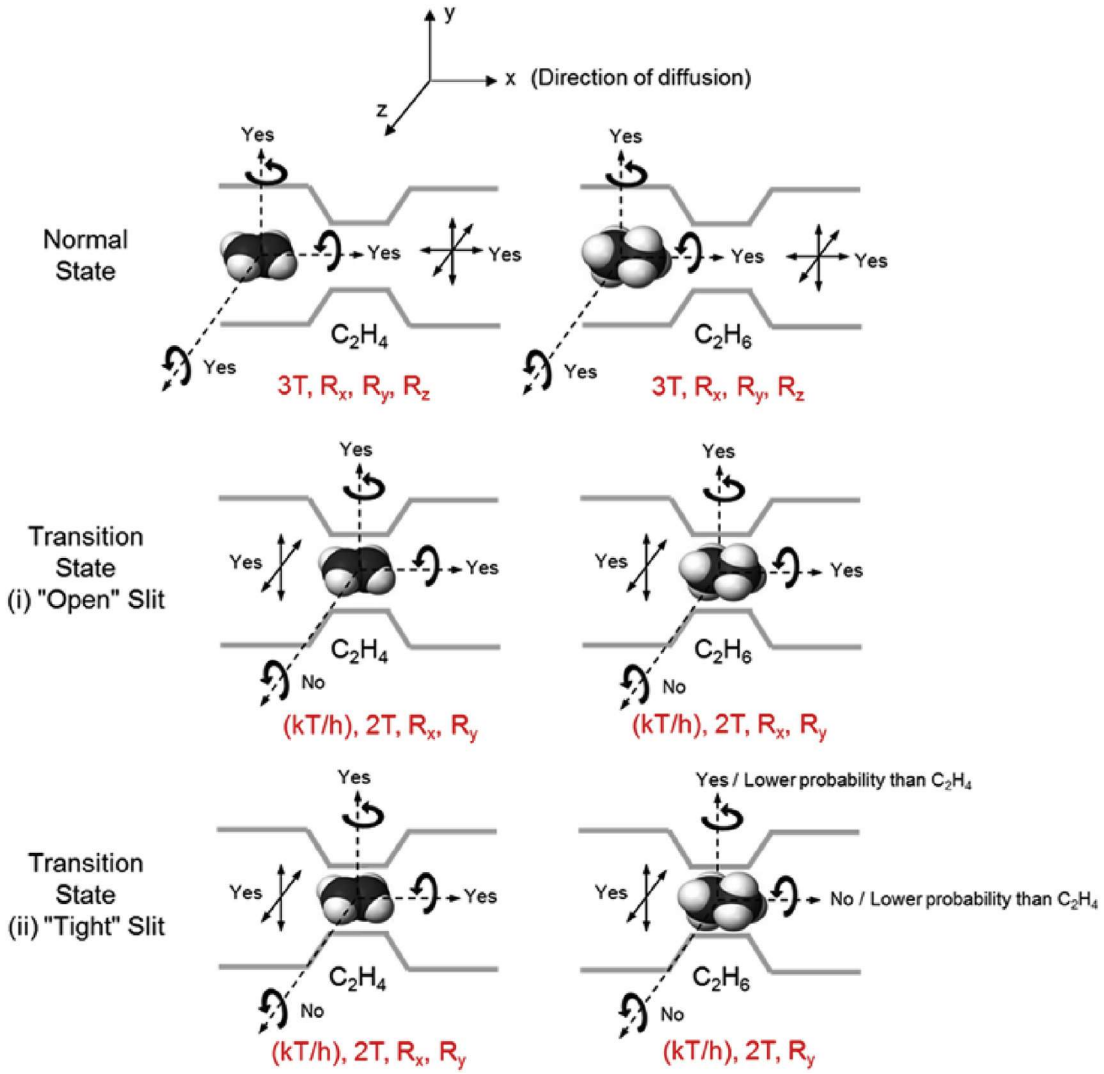

Fig. 6. Possible rotational and translational degrees of freedom options in: (i) "loose" and "tight" slit ultramicropores. Double-sided arrows indicate translational ability in the x, y or z directions (Adapted from Ref. [40]). (A colour version of this figure can be viewed online.)

~24 [38].

5. Ultrahigh selectivities enabled by synergistic entropic and sorption selectivities

A recent CMS selectivity-permeability tuning approach, based *only on adjusting pyrolysis temperature*, was recently reported by Zhang et al. [41] for Matrimid® derived CMS. Prior to this work, Matrimid® CMS membranes formed using pyrolysis temperatures above 800 °C were rarely reported. Zhang et al. explored effects of higher pyrolysis temperatures for 6 gas pairs (CO_2/CH_4, N_2/CH_4; O_2/N_2; He/CH_4; H_2/CH_4 and H_2/N_2) from 750 °C up to 900 °C, and all of the pairs showed extremely high permselectivities. Results are shown in Fig. 7 for N_2/CH_4 and He/CH_4 separation.

For example, the maximum entropically-enabled N_2/CH_4 diffusion selectivity has been estimated theoretically to be 52 [38]. The observed entropic selectivity (23.6) at 800 °C/UHP Argon was well below this theoretical maximum. Moreover, although the N_2 molecule is smaller, its more negative heat of sorption causes a higher diffusion activation enthalpy *vs.* CH_4. This feature makes the *energetic diffusion selectivity* term in Eq. (3) less than unity. Also, the unfavorable sorption selectivity ($\alpha_s < 1$) further offsets the favorable diffusive entropic selectivity for this pair. These combined factors make the permselectivity only ~8.0 at 800 °C/UHP Argon [38]. Zhang et al. found an overall N_2/CH_4 α_p ~63 for 900 °C/UHP Argon, in Fig. 7 [38]. This high N_2/CH_4 α_p was enabled by surprisingly high α_s = 2.2 at 900 °C/UHP Argon *vs* 0.75 at 800 °C/UHP Argon.

The increment in α_s was suggested to reflect exclusion of CH_4 from a fraction of micropore domains bounded by highly refined ultramicropores accessible to N_2 but not CH_4. An increase in diffusion selectivity was also observed (15 for 800 °C *vs.* 30 for 900 °C) reflecting an increase in energetic and entropic selectivities as well. As expected, CMS permeabilities are reduced at higher pyrolysis temperatures, due to effects discussed in terms of Fig. 3 related to tightening of both micropores and ultramicropores. This fact notwithstanding, these results illustrate a powerful tool to tune transport properties of CMS materials. Fig. 7c also shows another important application of this tuning approach wherein the strategically important He can be separated from CH_4. Indeed, with the extraordinarily high He/CH_4 α_p (~10,000 for 900 °C/UHP Argon pyrolysis), reasonably pure He product can be produced from even dilute He—CH_4 feeds.

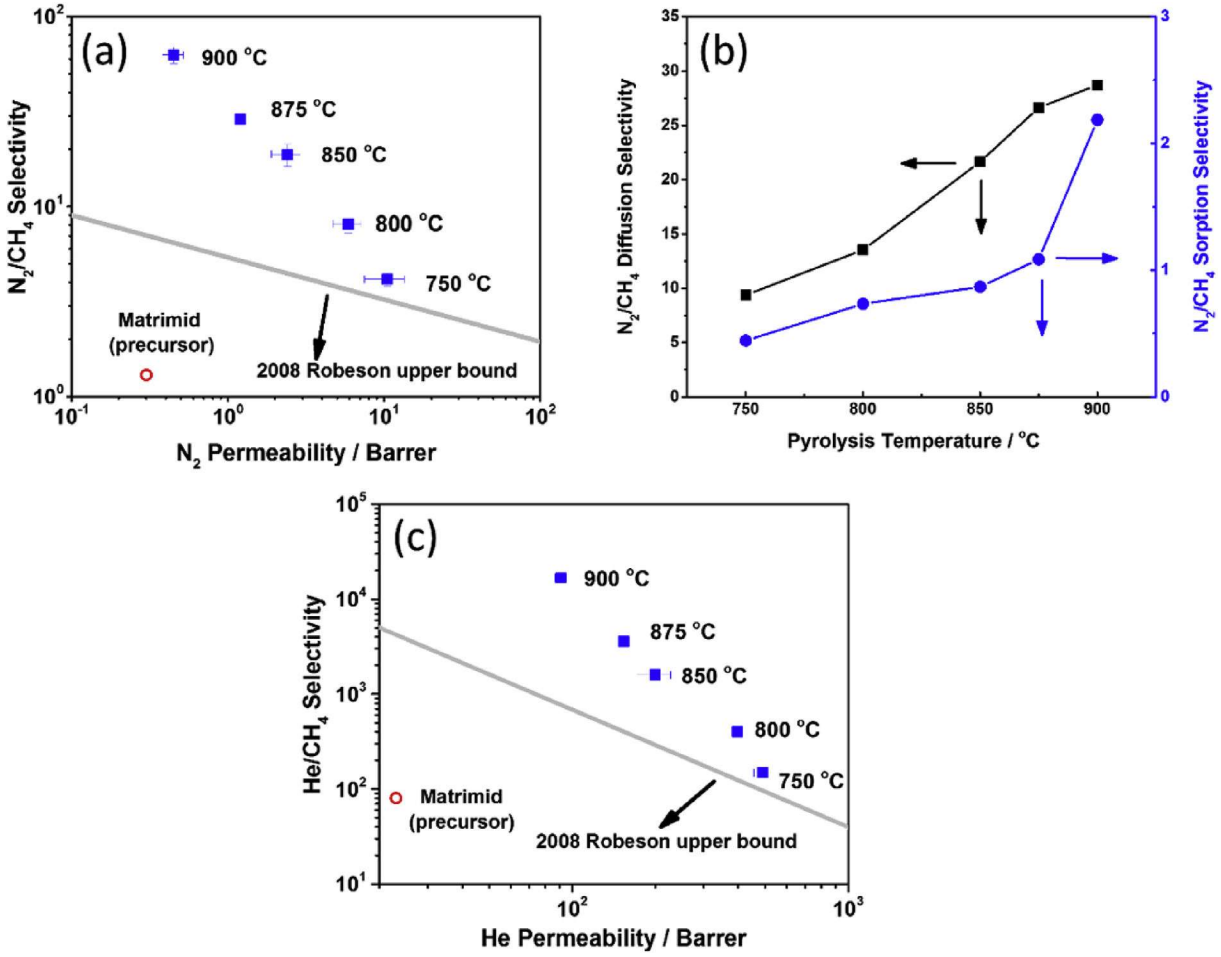

Fig. 7. (a). Matrimid® CMS N_2/CH_4 permselectivity (α_p) and N_2 permeability; (b) deconvolution of α_p into α_D and α_S and (c) He/CH_4 permselectivity (α_p) and He permeability (Reproduced with permission from Ref. [41]). (A colour version of this figure can be viewed online.)

6. Physical aging and its prevention for CMS materials

Like other disordered materials, post-pyrolyzed CMS materials can undergo physical aging [42], where partial densification of the imperfectly stacked plates may occur, with reduction in the *micropore size* illustrated in Fig. 8. This reduction in micropore size, as evident from decrease in sorption capacity results in permeability reduction [42].

This process shares features with physical aging of glassy polymers and inorganic glasses, since the disordered CMS is random over long ranges compared to individual organized plate structures comprising the micropore walls as shown in Fig. 3. On the other hand, a fundamental difference exists between simple glassy polymers *and CMS materials*, due to the lack of "thermo-reversibility" of the latter. Specifically, glassy and even liquid crystalline polymers display thermo-reversibility upon passing above their corresponding glass transition (T_g) or order-disorder temperatures (ODT) [27,43–46]. On the other hand, CMS materials are kinetically trapped quasi-ordered layered structures with a graphene-like ultimate end point. The kinetically trapped quasi-ordered structure with tunable permeation clearly depends upon the precursor and pyrolysis processes. Fortunately, CMS physical aging, which is apparent under vacuum storage, can be effectively "quenched". For instance in the case of CO_2/CH_4 by either maintenance of active feed to the membrane or simple storage under 100 psig CO_2 [47], the performance remains stable. This moderate pressure is equivalent to that in transported carbonated beverage bottles. Moreover, as shown in Fig. 9, the quenching of aging is effective even for the most open CMS material, 6FDA-DETDA:DABA (3:2). Alternative storage media that can effectively resist micropore tightening, without requiring higher pressures, would be valuable.

7. Translation of dense film to asymmetric CMS

Hollow fibers have higher packing density (area-per-volume) as compared to other membrane formats such as spiral wound and plate-and-frame modules; however, advantages of fibers *in CMS membranes* transcend such simple high surface-to-volume characteristics. Practical hollow fiber membranes maximize fluxes with *asymmetric morphologies* having a thin (0.5–5 μm) selective layer and microporous support layers. The cylindrical geometry in hollow fibers provides compressive shrinkage stresses that minimize potential processing defects during pyrolytic mass loss. Hollow fiber CMS membranes show flexibility illustrated in Fig. 10, which presumably reflects their primary sheet-like disturbed amorphous natures that allow deformations, not accommodated by crystalline zeolites or metal organic framework materials.

As shown schematically in Fig. 11, asymmetric precursor polymer structures actually have three layers, a dense molecularly selective layer, a mesoporous transition support layer, and a macroporous primary support layer. Asymmetric polymer

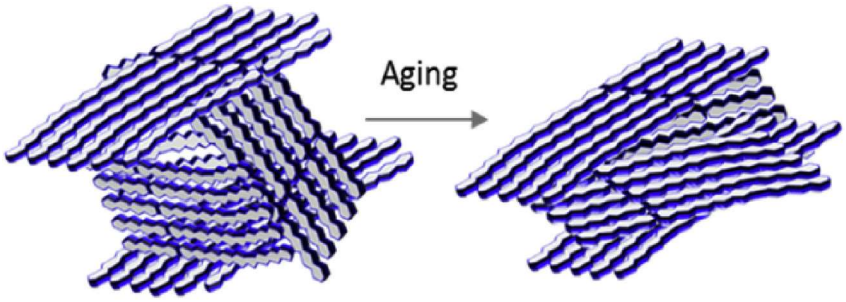

Fig. 8. Aging of CMS structure with micropore settling and minor ultramicropore slit tightening. (A colour version of this figure can be viewed online.)

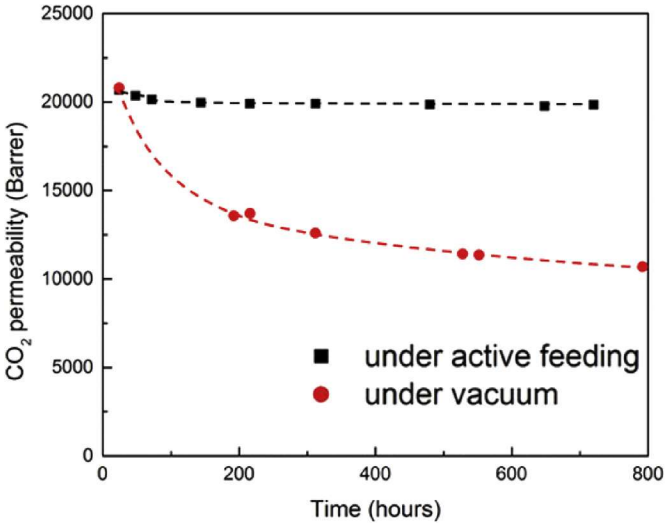

Fig. 9. Stability differences of 550 °C/UHP Argon pyrolyzed 6FDA-DETDA:DABA (3:2)-derived CMS under 50:50 CO_2:CH_4 50 psia active feed and 35 °C vs. sample stored under vacuum and tested periodically for 800 h. (A colour version of this figure can be viewed online.)

precursors are often represented simply as a two layer structure, with a skin on a porous support. The thin mesoporous transition layer is difficult to discern and is ideally "invisible" in terms of transport properties in the precursor. In the context of dense film to asymmetric translation, it is worthwhile to note the correlation

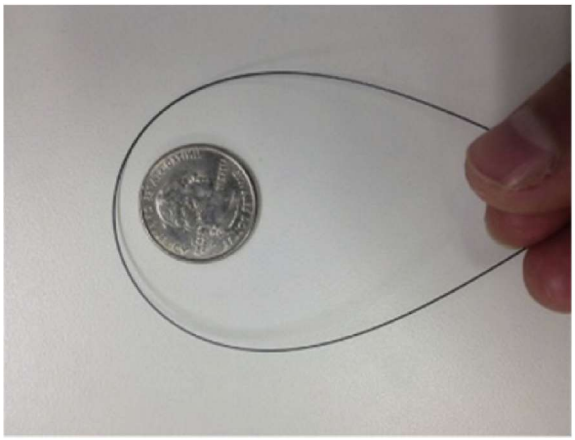

Fig. 10. Typical CMS fiber showing remarkable flexibility. (A colour version of this figure can be viewed online.)

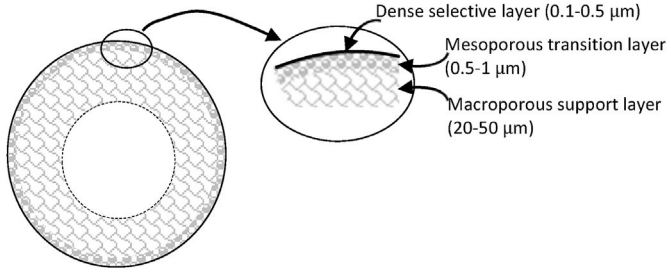

Fig. 11. Schematic of asymmetric precursor fiber.

between the "defect-free properties" of the precursor and the resulting CMS. In practice, a polymer precursor fiber is said to be "defect-free" if it's ideal selectivity for any given gas-pair is at least 90% of its corresponding dense film configuration selectivity. For a low molecular weight polymer like Matrimid®, pin-hole defects in the precursor fiber were healed during the pyrolysis process thereby forming defect-free asymmetric CMS. On the other hand, for more rigid, polymers like 6FDA:BPDA-DAM, spinning defect-free polymer precursors was found to be an absolute prerequisite for forming defect-free CMS [48].

Maintenance of an asymmetric hollow fiber under 100 psig CO_2 provides reasonably stable performance over a long time period, as shown by Wenz [47]. Fig. 12 shows permeance and selectivity trends for a 6FDA:BPDA-DAM 550 °C/UHP Argon CMS asymmetric fiber over 90 days. Over this time, the CMS membrane showed ~25%

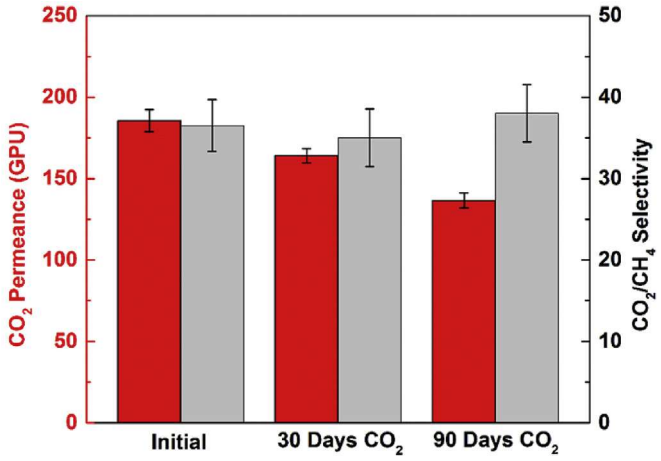

Fig. 12. Long-term stability test of asymmetric 6FDA: BPDA-DAM CMS when stored under 100 psig pure CO_2. Adapted from Ref. [47]. (A colour version of this figure can be viewed online.)

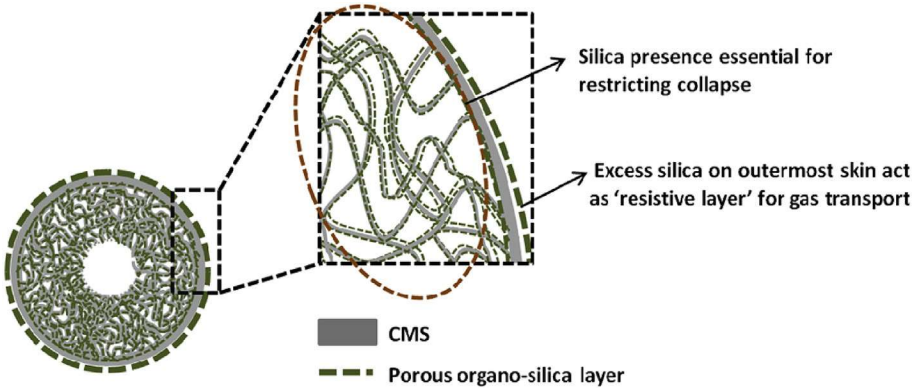

Fig. 13. Schematic representation of silica stabilization of an asymmetric CMS hollow fiber membrane (Reproduced with permission from Ref. [49]). (A colour version of this figure can be viewed online.)

drop in permeance and a 5% rise in selectivity, while still maintaining very attractive performance. The study by Xu et al. [42],showed that, as with glassy polymers, such aging effects are physical, rather than chemical in nature. Taken together, the results in Fig. 9 under active feed and results under CO_2 storage in Fig. 12 suggest physical aging is a manageable feature for CMS. While complete avoidance of physical aging would be desirable, as with amorphous glassy polymers, for the time being, the CO_2 storage method is an efficient and practical way to suppress physical aging when not under active feed.

8. Formation of thin-skinned hollow fibers

A reduced selective layer thickness in an asymmetric hollow fiber naturally leads to a more productive membrane. This can be achieved via a number of possible pathways like (i) starting with an ultrathin skinned defect-free asymmetric precursor which will also translate into an ultrathin skinned CMS fiber, or (ii) modification of existing precursors with >1 μm skin thickness to enable the formation of CMS fibers with a relatively thin skin. In this article, we focus more on the second approach, which involves a silica sol-gel stabilization method, as described in the following sections.

8.1. Sol-gel stabilization of asymmetric CMS

During the pyrolysis of asymmetric polymer fibers, preserving the asymmetry in the corresponding carbon membrane can be challenging. For relatively low glass transition temperature polyimides like Matrimid® ($T_g = 315\ ^\circ C$), the transition layer and porous support layer completely collapse upon heating beyond T_g. Several approaches, including precrosslinking of the structure were attempted, but did not provide true stabilization [48]. Bhuwania et al. [49] developed a silica sol-gel method that enables deposition of cross-linked porous silica on the porous struts of the support as illustrated in Fig. 13, *thereby mostly preventing collapse of the porous* support. The sol-gel deposition can be integrated into standard solvent exchange and drying steps, which are already used to stabilize asymmetric polymer structures, so minimal extra cost is involved [49]. For such asymmetric morphologies, the membrane productivity for a penetrant *A*, is usually expressed in terms of permeance (P_A/l) , which is essentially flux normalized over pressure (fugacity) driving force, as shown in Eq. (4).

$$\frac{P_A}{l} = \frac{N_A}{\Delta p_A} \tag{4}$$

This fact notwithstanding, if the porous support collapses, the permeance goes down.

Without sol-gel stabilization of a Matrimid® asymmetric precursor, Bhuwania et al. [49], observed complete collapse of the transition and macroporous support layers in the final CMS fiber. By using an optimized sol-gel treatment of the precursor with 10% Vinyl trimethoxy silane (VTMS) in hexane solution, the CMS skin layer was reduced from 40 to ~ 4–5 μm. A proportional increase of roughly 8X in CO_2 permeance reflected the 8.9X CMS selective layer thickness reduction from 40 μm to 4.5 μm, as seen approximately by SEM [49]. The agreement between SEM and transport results indicated that negligible added resistance arose from silica in this optimized VTMS deposition case. The higher T_g of the 6FDA:BPDA-DAM precursor in Table 1 (424 °C *vs.* 315 °C for Matrimid®), leads to an inherently lower tendency for collapse of the transition and macroporous layer, even without VTMS deposition. Bhuwania et al., extended the sol-gel method to 6FDA:BPDA-DAM precursor and a reduction in skin thickness from ~25 μm to ~2.5 μm, as seen by SEM, was achieved [49]. Studies to optimize VTMS concentrations for the 6FDA:BPDA-DAM precursor, as was done for Matrimid®, are underway.

Studies of sol-gel silica stabilized CMS *asymmetric* fibers reveal additional features that can affect transport properties beyond those present in dense CMS samples [49]. Specifically, the magnitude of a series transport resistance, added by a silica outer layer *on top of the selective CMS layer* depends upon transport properties of this silica layer relative to those of the CMS selective skin layer. Both sets of transport properties depend upon features of the sol-gel deposition and pyrolysis processes that create the silica and CMS layers, thereby requiring optimization of the process as well as of the precursor [50]. Even for sol-gel stabilized CMS membranes, during pyrolysis, the nonporous polymer skin layer tends to consolidate with the mesoporous transition layer to produce final CMS selective layers of 2.5–5 μm (exact thickness depends on the starting material). Such consolidated CMS selective layers are still much thinner with higher productivity than is the case without sol-gel reinforcement of the support.

9. Summary

The perspective we offered here had several objectives. One objective was to increase activity within the carbon community to use amorphous carbons as change agents to improve the state of the art in separation technology. Such activity is also an opportunity for characterization experts within our community. Indeed, CMS membranes provide ideal opportunities to characterization experts, since knowing the detailed nature of the precursor is a

requirement—not a luxury in membranes using these specialty carbons.

Capturing samples at different stages to probe permeation, diffusion and sorption properties as they undergo transformation from random coil amorphous materials to amorphous CMS is attractive. Even more attractive, however, would be using this information in conjunction with advanced characterization techniques on the same samples. This approach would help better test and improve understanding of the complex changes discussed in this article for specific precursors. This is especially appealing, since precursors can be tuned and tailored with exquisite control; however, the examples of the specific well-defined polymer precursors presented here would clearly be good starting points.

Our description of multiple, sometimes even simultaneous processes, outlined in this article, rely upon our knowledge of the traditional polymer field. Chain scissions under intense local stresses and entropically-driven self-assembly of complex spontaneously generated entities are known in different contexts in the polymer field. To help test these ideas, capturing and testing samples during the process for dense carbon samples would be valuable.

Sample capture of integrated higher order asymmetric fiber structures, while challenging, should also enable probing changes in the dense molecularly selective skin. Additional connections with the broader inorganic materials community to address pyrolysis and the parallel process of silica stabilization of the macroporous support are needed. Morphology stabilization during passage through the stage between the glass transition and the onset of carbonization goes beyond traditional carbon science per se; however, creating a functional molecular sieving material through carbon science remains the key requirement. Fortunately, the integrated steps to create a functional CMS membrane are not just a vision or a dream—they are a reality illustrated by examples discussed in this perspective. The first generation reality discussed here, however, needs refinement. This fact notwithstanding, to our knowledge, the parallel molecular scale processes discussed here allow achieving membranes with molecular discriminating capabilities that are *inaccessible by any other path that can be scaled into practical and economical membrane devices.*

Acknowledgements

The authors thank the Office of Basic Energy Science of the U.S. Department of Energy (DE-FG02-04ER15510) for financial support of this work.

References

[1] M. Varga, T. Izak, V. Vretenar, H. Kozak, J. Holovsky, A. Artemenko, M. Hulman, V. Skakalova, D.S. Lee, A. Kromka, Diamond/carbon nanotube composites: Raman, FTIR and XPS spectroscopic studies, Carbon 111 (2017) 54–61.
[2] S.A. Chernyak, A.S. Ivanov, K.I. Maslakov, A.V. Egorov, Z. Shen, S.S. Savilov, V.V. Lunin, Oxidation, defunctionalization and catalyst life cycle of carbon nanotubes: a Raman spectroscopy view, Phys. Chem. Chem. Phys. 19 (3) (2017) 2276–2285.
[3] J.-H. Zhou, Z.-J. Sui, J. Zhu, P. Li, D. Chen, Y.-C. Dai, W.-K. Yuan, Characterization of surface oxygen complexes on carbon nanofibers by TPD, XPS and FT-IR, Carbon 45 (4) (2007) 785–796.
[4] S.D. Gardner, C.S.K. Singamsetty, G.L. Booth, G.-R. He, C.U. Pittman, Surface characterization of carbon fibers using angle-resolved XPS and ISS, Carbon 33 (5) (1995) 587–595.
[5] T.I.T. Okpalugo, P. Papakonstantinou, H. Murphy, J. McLaughlin, N.M.D. Brown, High resolution XPS characterization of chemical functionalised MWCNTs and SWCNTs, Carbon 43 (1) (2005) 153–161.
[6] X.-y. Li, F. Tian, X.-p. Gao, F.-g. Bian, X.-h. Li, J. Wang, WAXD/SAXS study and 2D fitting (SAXS) of the microstructural evolution of PAN-based carbon fibers during the pre-oxidation and carbonization process, New Carbon Mater. 32 (2) (2017) 130–136.
[7] Z.Q. Li, C.J. Lu, Z.P. Xia, Y. Zhou, Z. Luo, X-ray diffraction patterns of graphite and turbostratic carbon, Carbon 45 (8) (2007) 1686–1695.
[8] B.N. Wang, R.D. Bennett, E. Verploegen, A.J. Hart, R.E. Cohen, Quantitative characterization of the morphology of multiwall carbon nanotube films by small-angle X-ray scattering, J. Phys. Chem. C 111 (16) (2007) 5859–5865.
[9] D. Lozano-Castelló, D. Cazorla-Amorós, A. Linares-Solano, Usefulness of CO 2 adsorption at 273 K for the characterization of porous carbons, Carbon 42 (7) (2004) 1233–1242.
[10] D. Cazorla-Amorós, J. Alcaniz-Monge, A. Linares-Solano, Characterization of activated carbon fibers by CO2 adsorption, Langmuir 12 (11) (1996) 2820–2824.
[11] K.-S. Liao, Y.-J. Fu, C.-C. Hu, J.-T. Chen, Y.-H. Huang, M. De Guzman, S.-H. Huang, K.-R. Lee, Y. Jean, J.-Y. Lai, Development of the asymmetric microstructure of carbon molecular sieve membranes as probed by positron annihilation spectroscopy, J. Phys. Chem. C 117 (7) (2013) 3556–3562.
[12] C.J. Anderson, S.J. Pas, G. Arora, S.E. Kentish, A.J. Hill, S.I. Sandler, G.W. Stevens, Effect of pyrolysis temperature and operating temperature on the performance of nanoporous carbon membranes, J. Membr. Sci. 322 (1) (2008) 19–27.
[13] L. Lajaunie, C. Pardanaud, C. Martin, P. Puech, C. Hu, M.J. Biggs, R. Arenal, Advanced spectroscopic analyses on a:C-H materials: revisiting the EELS characterization and its coupling with multi-wavelength Raman spectroscopy, Carbon 112 (2017) 149–161.
[14] Z. Wang, P. Poncharal, W. De Heer, Measuring physical and mechanical properties of individual carbon nanotubes by in situ TEM, J. Phys. Chem. Solids 61 (7) (2000) 1025–1030.
[15] K.M. Steel, W.J. Koros, Investigation of porosity of carbon materials and related effects on gas separation properties, Carbon 41 (2) (2003) 253–266.
[16] S. Fu, E.S. Sanders, S. Kulkarni, Y.-H. Chu, G.B. Wenz, W.J. Koros, The significance of entropic selectivity in carbon molecular sieve membranes derived from 6FDA/DETDA: DABA(3:2) polyimide, J. Membr. Sci. 539 (2017) 329–343.
[17] W. Qiu, L. Liu, W.J. Koros, Effect of block versus random copolyimide structure on hollow fiber membrane spinnability, J. Membr. Sci. 529 (2017) 150–158.
[18] H.O. Pierson, Handbook of Carbon, Graphite, Diamonds and Fullerenes: Processing, Properties and Applications, Noyes Publications, Park Ridge, NJ, 1993.
[19] S. Fu, E.S. Sanders, S.S. Kulkarni, W.J. Koros, Carbon molecular sieve membrane structure–property relationships for four novel 6FDA based polyimide precursors, J. Membr. Sci. 487 (2015) 60–73.
[20] M. Rungta, G.B. Wenz, C. Zhang, L. Xu, W. Qiu, J.S. Adams, W.J. Koros, Carbon molecular sieve structure development and membrane performance relationships, Carbon 115 (2017) 237–248.
[21] P.J. Williams, Analysis of Factors Influencing the Performance of CMS Membranes for Gas Separation, PhD Dissertation, Georgia Institute of Technology, 2006.
[22] A. Bürger, E. Fitzer, M. Heym, B. Terwiesch, Polyimides as precursors for artificial carbon, Carbon 13 (3) (1975) 149–157.
[23] G. Ehlers, K. Fisch, W. Powell, Thermal degradation of polymers with phenylene units in the chain. IV. Aromatic polyamides and polyimides, J. Polym. Sci. Part A Polym. Chem. 8 (12) (1970) 3511–3527.
[24] H. Hatori, Y. Yamada, M. Shiraishi, M. Yoshihara, T. Kimura, The mechanism of polyimide pyrolysis in the early stage, Carbon 34 (2) (1996) 201–208.
[25] M. Inagaki, S. Harada, T. Sato, T. Nakajima, Y. Horino, K. Morita, Carbonization of polyimide film “Kapton”, Carbon 27 (2) (1989) 253–257.
[26] M.J. Turk, A.S. Ansari, W.B. Alston, G.S. Gahn, A.A. Frimer, D.A. Scheiman, Evaluation of the thermal oxidative stability of polyimides via TGA techniques, J. Polym. Sci. Part A Polym. Chem. 37 (21) (1999) 3943–3956.
[27] P.J. Flory, Molecular Theory of Liquid Crystals, Liquid Crystal Polymers I, Springer, 1984, pp. 1–36.
[28] T.A. Centeno, J.L. Vilas, A.B. Fuertes, Effects of phenolic resin pyrolysis conditions on carbon membrane performance for gas separation, J. Membr. Sci. 228 (1) (2004) 45–54.
[29] A.M. Kratochvil, W.J. Koros, Decarboxylation-induced cross-linking of a polyimide for enhanced CO2 plasticization resistance, Macromolecules 41 (21) (2008) 7920–7927.
[30] S. Fu, G.B. Wenz, E.S. Sanders, S.S. Kulkarni, W. Qiu, C. Ma, W.J. Koros, Effects of pyrolysis conditions on gas separation properties of 6FDA/DETDA: DABA (3: 2) derived carbon molecular sieve membranes, J. Membr. Sci. 520 (2016) 699–711.
[31] M. Rungta, C. Zhang, W.J. Koros, L. Xu, Membrane-based ethylene/ethane separation: the upper bound and beyond, AIChE J. 59 (9) (2013) 3475–3489.
[32] X. Ma, R. Swaidan, B. Teng, H. Tan, O. Salinas, E. Litwiller, Y. Han, I. Pinnau, Carbon molecular sieve gas separation membranes based on an intrinsically microporous polyimide precursor, Carbon 62 (2013) 88–96.
[33] O. Salinas, X. Ma, E. Litwiller, I. Pinnau, Ethylene/ethane permeation, diffusion and gas sorption properties of carbon molecular sieve membranes derived from the prototype ladder polymer of intrinsic microporosity (PIM-1), J. Membr. Sci. 504 (2016) 133–140.
[34] M. Kiyono, P.J. Williams, W.J. Koros, Effect of pyrolysis atmosphere on separation performance of carbon molecular sieve membranes, J. Membr. Sci. 359 (1) (2010) 2–10.
[35] M. Kiyono, Carbon Molecular Sieve Membranes for Natural Gas Separations, PhD Dissertation, Georgia Institute of Technology, 2010.
[36] W.J. Koros, C. Zhang, Materials for next-generation molecularly selective synthetic membranes, Nat. Mater. 16 (3) (2017) 289–297.
[37] A. Singh, W. Koros, Significance of entropic selectivity for advanced gas separation membranes, Ind. Eng. Chem. Res. 35 (4) (1996) 1231–1234.
[38] X. Ning, W.J. Koros, Carbon molecular sieve membranes derived from

Matrimid® polyimide for nitrogen/methane separation, Carbon 66 (2014) 511–522.
[39] M. Rungta, L. Xu, W.J. Koros, Carbon molecular sieve dense film membranes derived from Matrimid® for ethylene/ethane separation, Carbon 50 (4) (2012) 1488–1502.
[40] M. Rungta, Carbon Molecular Sieve Dense Film Membranes for Ethylene/ethane Separations, PhD Dissertation, Georgia Institute of Technology, 2012.
[41] C. Zhang, W.J. Koros, Ultraselective carbon molecular sieve membranes with tailored synergistic sorption selective properties, Adv. Mater. 29 (33) (2017).
[42] L. Xu, M. Rungta, J. Hessler, W. Qiu, M. Brayden, M. Martinez, G. Barbay, W.J. Koros, Physical aging in carbon molecular sieve membranes, Carbon 80 (2014) 155–166.
[43] I.W. Hamley, M.D. Gehlsen, A.K. Khandpur, K.A. Koppi, J.H. Rosedale, M.F. Schulz, F.S. Bates, K. Almdal, K. Mortensen, Complex layered phases in asymmetric diblock copolymers, J. de Phys. II 4 (12) (1994) 2161–2186.
[44] Y. Huang, D.R. Paul, Experimental methods for tracking physical aging of thin glassy polymer films by gas permeation, J. Membr. Sci. 244 (1) (2004) 167–178.
[45] Y. Huang, X. Wang, D.R. Paul, Physical aging of thin glassy polymer films: free volume interpretation, J. Membr. Sci. 277 (1) (2006) 219–229.
[46] X. Wang, D.S. Miller, E. Bukusoglu, J.J. De Pablo, N.L. Abbott, Topological defects in liquid crystals as templates for molecular self-assembly, Nat. Mater. 15 (1) (2016) 106.
[47] G.B. Wenz, Tuning Carbon Molecular Sieve Membrane Performance for Challenging Gas Separations, PhD Dissertation, Georgia Institute of Technology, 2017.
[48] L. Xu, Carbon Molecular Sieve Hollow Fiber Membranes for Olefin/paraffin Separations, PhD Dissertation, Georgia Institute of Technology, 2012.
[49] N. Bhuwania, Y. Labreche, C.S. Achoundong, J. Baltazar, S.K. Burgess, S. Karwa, L. Xu, C.L. Henderson, P.J. Williams, W.J. Koros, Engineering substructure morphology of asymmetric carbon molecular sieve hollow fiber membranes, Carbon 76 (2014) 417–434.
[50] N. Bhuwania, Engineering the Morphology of Carbon Molecular Sieve (CMS) Hollow Fiber Membranes, PhD Dissertation, Georgia Institute of Technology, 2014.